

OSGIN1 is a novel TUBB3 regulator that promotes tumor progression and gefitinib resistance in non-small cell lung cancer

Xiaomeng Xie

Zhengzhou University

Kyle Vaughn Laster

China-US Hormel Cancer Institute

Jian Li

Zhengzhou University

Wenna Nie

China-US Hormel Cancer Institute

Yong Weon Yi

Dankook University

Kangdong Liu

Zhengzhou University

Yeon-Sun Seong

Dankook University

Zigang Dong

Zhengzhou University

Dong Joon Kim (✉ kjoon95@gmail.com)

China us hormel cancer institute <https://orcid.org/0000-0001-6910-9213>

Research Article

Keywords: OSGIN1, TUBB3, gefitinib resistance, NSCLC, patient-derived xenograft

Posted Date: May 3rd, 2023

DOI: <https://doi.org/10.21203/rs.3.rs-2826836/v1>

License:   This work is licensed under a Creative Commons Attribution 4.0 International License.

[Read Full License](#)

Version of Record: A version of this preprint was published at Cellular and Molecular Life Sciences on August 30th, 2023. See the published version at <https://doi.org/10.1007/s00018-023-04931-4>.

Abstract

Background

Oxidative stress induced growth inhibitor 1 (OSGIN1) regulates cell death. The role and underlying molecular mechanism of OSGIN1 in non-small cell lung cancer (NSCLC) are uncharacterized.

Methods

OSGIN1 expression in NSCLC samples was detected using immunohistochemistry and Western blotting. Growth of NSCLC cells and gefitinib-resistant cells expressing OSGIN1 or TUBB3 knockdown was determined by MTT, soft agar, and foci formation assays. The effect of OSGIN1 knockdown on *in vivo* tumor growth was assessed using NSCLC patient-derived xenograft models and gefitinib-resistant patient-derived xenograft models. Potentially interacting protein partners of OSGIN1 were identified using IP-MS/MS, immunoprecipitation, and Western blotting assays. Microtubule dynamics were explored by tubulin polymerization assay and immunofluorescence. Differential expression of signaling molecules in OSGIN1 knockdown cells was investigated using phospho-proteomics, KEGG analysis, and Western blotting.

Results

We found that OSGIN1 is highly expressed in NSCLC tissues and is positively correlated with low survival rates and tumor size in lung cancer patients. OSGIN1 knockdown inhibited NSCLC cell growth and patient-derived NSCLC tumor growth *in vivo*. Knockdown of OSGIN1 strongly increased tubulin polymerization and re-established gefitinib sensitivity *in vitro* and *in vivo*. Additionally, knockdown of TUBB3 strongly inhibited NSCLC cell proliferation. Mechanistically, we found that OSGIN1 enhances DYRK1A-mediated TUBB3 phosphorylation, which is critical for inducing tubulin depolymerization. The results of phospho-proteomics and ontology analysis indicated that knockdown of OSGIN1 led to reduced propagation of the MKK3/6-p38 signaling axis.

Conclusions

We propose that OSGIN1 modulates microtubule dynamics by enhancing DYRK1A-mediated phosphorylation of TUBB3 at serine 172. Moreover, elevated OSGIN1 expression promotes NSCLC tumor growth and gefitinib resistance through the MKK3/6-p38 signaling pathway. Our findings unveil a new mechanism of OSGIN1 and provide a promising therapeutic target for NSCLC treatment in the clinic.

Background

Despite the significant advances achieved in cancer therapeutics, lung cancer remains one of the most malignant tumors worldwide, with a 5-year survival lower than 20% [1]. The high incidence and mortality of lung cancer are due to unknown molecular mechanisms governing disease progression and the lack of effective therapeutic strategies [2]. Developing a more comprehensive understanding of NSCLC and its

related risk factors can enable the discovery of drugs tailored to target critical networks that drive lung cancer development. With respect to lung cancer incidence, non-small cell lung cancer (NSCLC) (including lung squamous cell carcinoma, lung adenocarcinoma, and large cell carcinoma) patients comprise approximately 85% of cases [3]. Therefore, exploring the molecular mechanisms contributing to NSCLC development have become an important task and prerequisite for conquering NSCLC.

Oxidative stress plays an important role as a secondary messenger in the regulation of various physiological processes, including apoptosis, survival, and cellular proliferation [4]. Importantly, oxidative stress can facilitate tumor formation by modifying the structure and function of critical cellular macromolecules including DNA resulting in cell growth, mutation, and/or chromosome instability [5]. The *OSGIN1* (also known as OKL38) gene encodes an oxidative stress response protein that regulates cell death by inducing cytochrome c release from mitochondria [6]. OSGIN1 is absent or expressed at low levels in a variety of malignant tumors, including breast cancer, kidney cancer, and liver cancer. Moreover, lower OSGIN1 levels are closely related to worse patient prognosis [7–9]. Additionally, it has also been reported that hepatocellular carcinoma patients harboring a specific OSGIN1 variation (NT1494: G-A) had shorter survival times [10]. Meanwhile, it was previously reported that both up- and down-regulation of OSGIN1 could enhance autophagy response induced by tobacco smoking in the human airway epithelium [11]. Additionally, silencing of OSGIN1 inhibited cell migration by regulating autophagy upon palmitic acid treatment [12]. Taken together, the biological function of OSGIN1 needs to be further elucidated and its role in NSCLC is poorly characterized.

TUBB3 (tubulin beta 3 class III) belongs to β -tubulin family. α - and β -tubulin heterodimers can combine to form hollow cylindrical microtubules that continuously elongate and shorten during all phases of the cell cycle [13, 14]. Alterations in microtubule formation are thought to influence cellular responses to chemotherapy and microenvironmental stressors, thereby contributing to broad-spectrum chemotherapy resistance, tumor development, and cell survival [15]. TUBB3 is associated with microtubule dynamics and impairs the effect of drugs that interfere with microtubule polymerization by increasing microtubule dynamic instability [16–18]. TUBB3 was reported to promote tumorigenesis and anoikis resistance through PTEN/AKT signaling in NSCLC [19]. Targeting the IL-1 β /EHD1/TUBB3 axis was shown to overcome gefitinib resistance in NSCLC [20]. It was previously reported that phosphorylation of β -tubulin Ser172 precludes the incorporation of tubulin dimers into microtubules, thus downregulating microtubule polymerization [21]. Phosphorylation of any β -tubulin isotype at Ser172 by CDK1 or DYRK1A impedes the incorporation of tubulin dimers into microtubules, thus reducing overall dimer availability and inducing microtubule depolymerization [22]. Therefore, the alteration of microtubule dynamics through TUBB3 may be associated with cancer progression and gefitinib resistance in NSCLC.

In this study, we uncover novel oncogenic functions of OSGIN1 that contribute to microtubule dynamics through DYRK1A-mediated TUBB3 phosphorylation in NSCLC. OSGIN1 may serve as a potential therapeutic target against NSCLC.

Methods

Reagents and antibodies

Cell culture media, gentamicin, penicillin, and L-glutamine were all obtained from Invitrogen (Grand Island, NY, USA). Tris, NaCl, and SDS for molecular biology and buffer preparation were purchased from Sigma-Aldrich (St. Louis, MO, USA). Antibodies to detect OSGIN1 (15248-1-AP) and GAPDH (HRP-60004) were purchased from Proteintech (Wuhan, Hubei, China). β -Actin (sc-47778), GST (sc-138), His-HRP (sc-8036HRP) antibodies were purchased from Santa Cruz Biotechnology, Inc. (Santa Cruz, CA, USA). Anti-Flag (F1804) was purchased from Sigma-Aldrich (St. Louis, MO, USA). Antibodies to detect Myc (2276), TUBB3 (5568), DYRK1A (8765), MKK3 (8535), MKK6 (8550), p-MKK3/6 (12280), p38 (8690), p-p38 (9211) were purchased from Cell Signaling Technology (Danvers, MA, USA). P-TUBB3 (ab76286) antibodies were purchased from Abcam (Chembridge Science Park, Chembridge, UK).

Construction of expression vectors

Expression constructs, including Myc-OSGIN1, Flag-OSGIN1, Flag-TUBB3 were obtained from GeneCopoeia (USA). Additionally, the lentivirus plasmids shOSGIN1 (#2, 5'-CCGGGGGACAACTTCGTGAGGTTTGCTCGAGCAAACCTCACGAAG

**TTGTCCCTTTTTG-3', #7, 5'-
CCGGGGACTTAGACCAGTGTCTGAGCTCGAGC**

TCAGACACTGGTCTAAGTCCTTTTTG - 3') were designed using the Invitrogen BLOCK-iT™ RNAi Designer. The pLKO.1-puro non-target shRNA Control Plasmid DNA (shControl) was purchased from Sigma-Aldrich (St. Louis, MO, USA). All constructs were confirmed by restriction enzyme mapping, DNA sequencing, alignment using the BLAST program.

Cell culture and transfection

Human lung cancer cell lines (A549, H460, H1299, H1650) and the human bronchial epithelial cell NL20 were obtained from the Cell Bank of the Chinese Academy of Sciences (Shanghai, China). Human lung cancer cell lines were cultured in RPMI-1640 medium supplemented with 10% fetal bovine serum (FBS; Biological Industries, Cromwell, CT, USA) and 1% antibiotic-antimycotic. NL20 cells were cultured in Ham's F12 supplemented with 0.324 g/L sodium bicarbonate, 0.9 g/L glucose, 1 mM L-glutamine, 0.1 mM non-essential amino acid, 5 μ g/ml insulin, 10ng/ml EGF, 1 μ g/ml transferrin, 500 ng/ml hydrocortisone, 4% FBS and 1% antibiotic-antimycotic in a 37°C humidified incubator under a 5% CO₂ atmosphere. Cells were cytogenetically tested and authenticated before expansion, freezing, and storage in liquid nitrogen. Each cell line was maintained in culture for a maximum of 8 weeks. Transfections were performed using Lipo2000 Transfection Reagent (Invitrogen, Grand Island, NY, USA) following the manufacturer's instructions when cells reached 60% confluence. The cells were cultured for 48 h and proteins were extracted for further analysis.

Lentiviral infection

Lentiviral expression vectors of OSGIN1/TUBB3 (shOSGIN1/shTUBB3) or the *pLKO.1-puro* non-target shRNA Control Plasmid DNA (shControl) and packaging vectors (*pMD2.0G* and *psPAX2*) were transfected into Lentix-293T cells using the Lipo2000 transfection reagent following the manufacturer's instructions. Briefly, the transfection mixture in 10% FBS/DMEM without antibiotics was incubated with cells for 4–6 h. Afterward, the media was discarded and replaced with 10 mL of fresh complete DMEM medium with antibiotics (penicillin/streptomycin). Viral supernatant fractions were collected after 48 h and filtered through a 0.45 µm syringe filter. The filtered virus-enriched media was then supplemented with 10 µg/mL polybrene (Millipore, Billerica, MA) and applied to the target cells. After infection for 48 h, the medium was discarded and replaced with fresh complete growth medium containing the appropriate concentration of 1 µg/mL puromycin. The cells were selected in puromycin for an additional 48 h. The selected cells were used for subsequent experiments.

Cell based assays: cell viability, colony formation, foci formation

For cell proliferation assays, 2×10^3 cells/well were seeded in 96-well plates and incubated for different time (0, 24, 48 or 72 h) to measure cell proliferation by MTT assay. For anchorage-independent colony formation assays, cells (8×10^3 cells/well) were suspended in complete medium supplemented with 0.3% agar in a top layer over a bottom layer supplemented with 0.6% agar in 6-well plates. The plates were maintained in a 37°C humidified incubator under a 5% CO₂ atmosphere for 1 to 2 weeks. For foci formation assays, 500–800 cells/well were seeded in 6-well plates and incubated for 10 to 14 days. The foci were subsequently stained with 0.4% crystal violet and photographed using a camera-mounted wide-field microscope.

Quantitative real-time PCR

OSGIN1 knockdown and control NSCLC cells (1×10^6) were plated into 100-mm dishes, cultured overnight, and then harvested. An RNA extraction kit (Invitrogen, Grand Island, NY, USA) was used for total RNA extraction. OSGIN1 gene expression was analyzed with 15 ng of total RNA. After cDNA synthesis (Vazyme, Nanjing, China), cDNA was amplified by quantitative one-step real-time PCR following the manufacturer's suggested protocols. The OSGIN1-specific real-time primers used for RNA quantification are as follows: F: 5'- GCCTGGCACTCCATCGAAG – 3'; R: 5'- TGACCACGTAGTCCCTGTAGTA – 3'. The TUBB3-specific real-time primers used for RNA quantification are as follows: F: 5'- GGAGGCACCTCAGACACTCA – 3'; R: 5'- CGATGCCATGCTCATCACTG – 3'. The CT values of OSGIN1 gene expression were normalized with the CT values of actin as an internal control to ensure equal RNA utilization.

Western blotting

Protein concentration were measured by BCA kit (solarbio, Beijing, China) following the manufacturer's suggested protocol. Proteins were separated by SDS/PAGE and transferred to polyvinylidene difluoride membranes (Amersham Biosciences, Piscataway, NJ, USA). After blocking with 5% nonfat dry milk at room temperature for 1 h, membranes were then incubated overnight with the appropriate primary antibodies at 4°C. The next day, the membranes were washed three times with TBST before and after incubation with 1:10000 dilution of horseradish peroxidase-linked secondary antibody for 1h. The immuno-reactive proteins were detected with chemiluminescence reagent (New Cell Molecular Biotech, Suzhou, China) using the ImageQuant LA S4000 system (GE Healthcare, Piscataway, NJ, USA).

Tubulin polymerization assay

Lung cancer cells stably expressing shControl or shOSGIN1 were grown in 60-mm plates for 24 h. Afterward, the cells were harvested after washing twice with PBS and then disrupted with 100 µl hypotonic buffer (0.5% NP40, 2 mM EGTA, 1 mM MgCl₂, 20 mM Tris-HCl pH 6.8, and a protease inhibitor mixture) for 15 min at room temperature. The lysates were subsequently centrifuged at 13,000 rpm for 15 min at 4°C. After measuring the total protein concentration using a BCA kit (Solarbio, Beijing, China), the soluble fraction containing depolymerized tubulin was separated from the insoluble fraction containing polymerized tubulin. Each fraction was mixed with equal volumes of 5 × SDS loading buffer, heated for 5 min at 95°C, and analyzed by Western blotting.

Surface plasmon resonance (SPR)

SPR assay was performed according to the instructions provided with the Biacore T200 (GE Healthcare, England, UK) instrument. OSGIN1 protein was immobilized onto a CM5 sensor chip. Next, the chip was equilibrated with PBS. A concentration series of TUBB3 protein were added into the flow system to test the binding affinity between TUBB3 and OSGIN1. TUBB3 was dissolved in PBS and perfused onto the CM5 chip at a 30 µl/min flow rate; 120 sec contact time and 300 sec dissociation time were set as the additional parameters. The T200 evaluation state model was utilized to analyze the binding affinity data and calculate the protein's K_D value. Representative curves were re-plotted using the GraphPad Prism software.

In vitro kinase assay

The kinase assay was performed according to the instructions provided by Upstate Biotechnology (Billerica, MA, USA). Active recombinant DYRK1A (100 ng), TUBB3 (300 ng) or OSGIN1 (25, 100 ng) proteins were mixed with ATP and incubated at 30°C for 30min. The reactions were terminated by adding 5 µl protein loading buffer. Afterward, the mixtures were separated by SDS-PAGE. DYRK1A activity was evaluated using an antibody directed against TUBB3 phosphorylated at serine 172.

Co-immunoprecipitation assay

Cells were co-transfected with OSGIN1-Myc and TUBB3-Flag plasmids. After transfection for 48 h, cell pellets were harvested and incubated with lysis buffer (50 mM Tris-HCl pH 7.4, 1 mM EDTA, 1% TritonX-100, 150 mM NaCl) supplemented with protease inhibitors for 1 h at 4°C. After quantification, appropriate cell lysates were incubated with beads containing specific tags and rotated overnight at 4°C. The next day, the beads were washed four times with washing buffer (20 mM HEPES pH 7.9, 0.1 M KCl, 0.1 M NaCl, 5 mM EDTA pH 8.0, 0.5% NP40) supplemented with protease inhibitors. The immune complexes were subsequently eluted at 95°C for 5 min with 5× loading buffer. Finally, the immunoprecipitated complexes were visualized by Western blotting.

Immunohistochemistry

The slides containing tissue sections were baked at 65°C for 3 h. After de-paraffinization and hydration, slides were boiled in citrate buffer for 90 sec at a high temperature and pressure. Slides were then treated with H₂O₂ for 5 min, and incubated with primary antibody at 4°C overnight. Slides were stained with DAB (3, 3'-diaminobenzidine) after incubation with the appropriate secondary antibody. The immunohistochemistry staining was quantified by calculating the integrated optical density (IOD) value measured by Image-Pro Plus analysis.

Immunofluorescence

Cells were grown in a 24-well plate atop 15 mm circle microscope glass coverslips (NEST, USA). After washing the coverslips three times with PBS, samples were fixed in 100% methanol for 15 min. The samples were then blocked with 3% BSA at room temperature for 1 h. Afterward, the coverslips were then incubated with appropriate primary antibodies overnight at 4°C. The next day, the coverslips were washed with PBS before and after incubation with a 1:1000 dilution of the appropriate secondary antibody for 1 h. The cells were then counterstained with DAPI and mounted onto glass microscope slides. Immunofluorescence images were photographed using a Nikon A1R confocal microscope.

Pull down assay and mass spectrometry

Myc beads were incubated with H1299 lysates (Myc-OSGIN1 transfected only and pcDNA 3.1 vector transfected only as control) for 16 h at 4°C. The samples were then washed four times in washing buffer (20 mM HEPES pH 7.9, 0.1 M KCl, 0.1 M NaCl, 5 mM EDTA pH 8.0, 0.5% NP40) supplemented with protease inhibitors and then subjected to SDS/PAGE. Using CBB staining, discrepant gel lanes were cut down and prepared for mass spectrometry.

Phosphoproteomics

Lysates of cells stably expressing shControl or shOSGIN1 #7 were used for phosphorylated proteomics. The TiO₂-enrichment method was used to analyze phosphoproteomics [23].

Computer modeling

The three-dimensional (3D) structures of TUBB3 and DYRK1A are obtained from the Protein Data Bank (PDB Accession Number 6S8L and 2WO6, respectively). DYRK1A is known to phosphorylate TUBB3 at Ser172. Therefore, the DYRK1A catalytic residue Asp287 was specified to be within 8Å to the TUBB3 Ser172 in the docking process. The DYRK1A-TUBB3 model with the best docking score was chosen as the receptor molecule to further dock OSGIN1 onto it. Since OSGIN1 does not have an experimentally defined structure, AlphaFold model (AF-Q9UJX0-F1-model_v4) was used. The final model is consistent with experimental data and has a docking score < -200, which is similar to the values of complex structures in the PDB, indicating a high-confidence model.

Patient-derived lung tumor xenografts (PDX)

Severe combined immunodeficiency (SCID) female mice (6–9 weeks old) (Cyagen, Santa Clara, USA) were maintained under “specific pathogen-free” conditions based on the guidelines established by the Zhengzhou University Institutional Animal Care and Use Committee. Human lung tumor specimens were obtained from the Affiliated Cancer Hospital in Zhengzhou University. Tissues were cut into small pieces and inoculated into the back of the neck of each mouse. Mice were divided into 3 groups consisting of 7–8 animals/group for the HLG77 and HLG80 PDX models as follows: 1) shControl virus infected group; 2) shOSGIN1 #2 virus infected group and 3) shOSGIN1 #7 virus infected group. Previously, an in vivo gefitinib-resistant NSCLC PDX model (LG1GR) was generated in-house [24]. Mice were divided into 4 groups consisting of 7 animals/group for the LG1GR PDX model as follows: 1) shControl virus infected group; 2) shControl virus infected + 50 mg/kg gefitinib group; 3) shOSGIN1 #2 virus infected group and 4) shOSGIN1 #2 virus infected + 50 mg/kg gefitinib group. shControl and shOSGIN1 virus were injected 3 times over the course of 10 days. The gefitinib treatment regimen was initiated when the tumor volume reached approximately 300 mm³. Tumor volume was calculated from measurements of 2 diameters of the individual tumor base using the following formula: tumor volume (mm³) = (length × width × height × 0.52). Mice were monitored until tumors reached approximately 1.5 cm³ total volume, at which time the mice were euthanized and the tumor tissues, liver, kidney and spleen were extracted.

Databases and online survival analysis platform

The expression of TUBB3 in lung adenocarcinoma is obtained from the ualcan website (<https://ualcan.path.uab.edu/index.html>) [25] and the survival rate is analyzed using Kaplan-Meier Plotter (<http://kmplot.com/analysis>) [26]. The results of phosphoproteomics was investigated using KEGG (<http://www.kegg.jp>) [27].

Statistical analysis

All quantitative results were expressed as mean values \pm S.D. or \pm S.E. Significant differences were compared using the Student's t test, nonparametric test or one-way analysis of variance (ANOVA). A p value of < 0.05 was considered to be statistically significant. The statistical package for social science (SPSS) for Windows (IBM, Inc. Armonk, NY, USA.) was used to calculate the p value to determine statistical significance.

Results

OSGIN1 expression is elevated in NSCLC and is a negative prognostic factor for NSCLC patients

To examine the expression status of OSGIN1 in NSCLC, we first conducted immunohistochemical assays to determine the relative OSGIN1 protein expression levels in normal lung, adjacent, and NSCLC tissues collected from 55 patients at the Affiliated Cancer Hospital of Zhengzhou University. OSGIN1 protein expression was significantly increased in NSCLC tissues compared to levels observed in adjacent tissues and normal tissues (Fig. 1A). To further assess the potential role of OSGIN1 in NSCLC, we once again utilized immunohistochemical to measure its expression in 85 paired NSCLC tissues and adjacent tissues included in a tissue array. Our results showed that OSGIN1 was significantly overexpressed in NSCLC tissues compared to the paired adjacent tissues (Fig. 1B). Furthermore, we assessed OSGIN1 expression by qRT-PCR and Western blotting in normal lung and NSCLC cell lines. Our findings indicated that NSCLC cells exhibited increased OSGIN1 mRNA and protein levels compared with NL20 normal lung cells (Fig. 1C, D). Moreover, Kaplan–Meier analysis[28] showed that patients with high levels of OSGIN1 exhibited a lower survival probability (Fig. 1E). In addition, correlation analysis of the patient clinical information revealed that OSGIN1 expression was positively correlated with tumor size (Fig. 1F).

OSGIN1 promotes growth of non-small cell lung cancer in vitro and in vivo. To investigate the role of OSGIN1 in NSCLC cells, we generated two OSGIN1 knockdown NSCLC cell lines (Supplementary Fig. 1A, B). We next performed MTT and soft agar assays to assess alterations in cell proliferation in response to OSGIN1 knockdown. We found that anchorage-dependent and -independent NSCLC cell growth were significantly decreased upon OSGIN1 knockdown (Fig. 2A, B). To further confirm the effect of ectopic OSGIN1 expression on NSCLC cell growth, we established stable OSGIN1 expressing H1299 and H1650 cells; ectopic protein expression was subsequently confirmed by Western blotting (Supplementary Fig. 1C). MTT and soft agar results showed that the growth of NSCLC cells ectopically expressing OSGIN1 was significantly increased compared to that of control cells (Fig. 2C, D). Furthermore, to investigate whether OSGIN1 knockdown can inhibit NSCLC tumor growth *in vivo*, we established NSCLC patient-derived xenograft (PDX) mouse models. The volume and growth rate of tumors in shOSGIN1 injected mice were significantly decreased compared to shControl injected mice (Fig. 2E). Moreover, the average body weight of mice did not differ significantly between the control and experimental groups

(Supplementary Fig. 2A, B). Tumor size and the average tumor weight in the shOSGIN1 injected mice groups was much smaller than those in the shControl injected mice group (Fig. 2F). Western blotting analysis of tumor tissues confirmed lower OSGIN1 protein levels in tumor tissues with a lower growth rate (Fig. 2G). These results illustrate that OSGIN1 promotes aberrant cell proliferation and plays an important role in NSCLC tumor growth *in vitro* and *in vivo*.

OSGIN1 directly binds to TUBB3

Previously, it was reported that a variation in the OSGIN1 nucleic acid sequence (NT1494: G-A) affected the transport of OSGIN1 from the nucleus to the mitochondria, thereby reducing the ability of OSGIN1 to promote apoptosis in hepatocellular carcinoma [10]. Therefore, we investigated whether OSGIN1 is a nucleotide variation in NSCLC. OSGIN1 was fully sequenced in NL20 normal lung cells and NSCLC cells. Our results indicated that the indicated cell lines harbored no variations in the full length OSGIN1 nucleic acid sequence (data not shown). We next conducted mass spectrometry analysis to explore OSGIN1-interacting proteins to elucidate potential molecular mechanisms involving OSGIN1 in NSCLC (Supplementary Fig. 3). Potentially interacting proteins with OSGIN1 were identified based on the MS score results; the top priority protein was found to be TUBB3 according to the MS score. (Supplementary table 1). To confirm the interaction between OSGIN1 and TUBB3, we performed co-immunoprecipitation assays using lysates derived from H1299 cells expressing OSGIN1 and/or TUBB3. Flag-TUBB3 was found to precipitate Myc-OSGIN1 from H1299 cell lysates; similarly, OSGIN1 was also found to bind with TUBB3 (Fig. 3A). Furthermore, we validated the direct interaction between OSGIN1 and TUBB3 using recombinant proteins (Fig. 3B). In addition, SPR assay results calculated a KD value of 144.2 nM between the proteins (Fig. 3C). To investigate the structural regions that mediate the physical interaction between OSGIN1 and TUBB3, we constructed deletion mutants of OSGIN1 and TUBB3. We identified that the OSGIN1 was mostly responsible for mediating the interaction with TUBB3 (data not shown). Additionally, we found that the M2 region (1-215 amino acid fragment) of TUBB3 was responsible for mediating the interaction with OSGIN1 (Fig. 3D).

TUBB3 regulates NSCLC growth and is correlated with lung cancer patient survival rates

To examine the functional significance of TUBB3 in lung cancer, we analyzed TUBB3 mRNA expression levels in NSCLC and normal lung tissues using RNA-seq data provided by The Cancer Genome Atlas (TCGA). The results indicated that TUBB3 mRNA levels were significantly increased in NSCLC tissues compared to normal lung tissues (Fig. 4A). Additionally, Western blotting analysis revealed increased TUBB3 protein expression levels in NSCLC cells compared to those observed in NL20 normal epithelial cells (Fig. 4B). Furthermore, the Kaplan–Meier plotter online tool was used to assess the potential significance of TUBB3 expression on lung cancer survival. The results consistently indicated that NSCLC patients with elevated levels of TUBB3 expression exhibited poorer overall survival ($P = 6.7e-16$) than corresponding patients with low TUBB3 expression levels (Fig. 4C). To determine the effect of TUBB3

knockdown on NSCLC growth, we established TUBB knockdown cells and validated protein expression by Western blotting (Supplementary Fig. 4A). The results of MTT and soft agar assays indicated that depletion of TUBB3 inhibited NSCLC cell growth and colony formation (Fig. 4D, E). Next, the effect of overexpressing TUBB3 on the NSCLC cell growth was determined. Thus, we next established H1650 cells stably expressing TUBB3 (Supplementary Fig. 4B). MTT assay and colony formation assay results consistently showed that TUBB3 induced NSCLC cell growth and colony formation (Fig. 4F, G). Taken together, these results suggest that TUBB3 promotes NSCLC cell growth.

Suppression of OSGIN1 increases TUBB3 precipitation and represses the MKK3/6-p38 signaling pathway

As TUBB3 plays an important role in microtubule assembly, we investigated whether TUBB3 could affect the supernatant and precipitate ratio upon OSGIN1 knockdown. Results indicated that TUBB3 precipitation was dramatically increased (Fig. 5A). In addition, we investigated microtubule morphology by immunofluorescence and found that inhibition of OSGIN1 induced increased tubulin polymerization (Fig. 5B). Next, we utilized TiO₂-enriched phospho-proteomics to determine the molecular mechanism of OSGIN1 (Fig. 5C, Supplementary table 2). We then investigated cancer-related signaling using KEGG pathway enrichment and identified that components of the MAPK signaling pathway were mostly affected in cells with altered OSGIN1 protein expression levels (Fig. 5D). Among the proteins involved in MAPK signaling pathway, we observed that those specifically enriched in the JNK and p38 signaling pathway were extremely significant. Therefore, we performed Western blotting to verify alterations in the JNK and p38 signaling pathways. Results showed that OSGIN1 knockdown consistently inhibited p-MKK3/6 and p-p38 expression, but not JNK signaling (Fig. 5E, Supplementary Fig. 5). Notably, similar changes in the MKK3/6-p38 axis were observed in TUBB3 knockdown cells (Fig. 5F). Taken together, these results suggest that suppression of OSGIN1 induces tubulin polymerization and downregulates MKK3/6-p38 signaling.

OSGIN1 promotes phosphorylation of TUBB3 at serine 172 by DYRK1A via enhanced interaction between DYRK1A and TUBB3

Next, we investigated whether OSGIN1 knockdown could affect protein modification and expression of TUBB3. We found that OSGIN1 knockdown led to decreased phosphorylation of TUBB3 at serine 172; however, no obvious effect on TUBB3 expression at the mRNA and protein level were observed (Fig. 6A; Supplementary Fig. 6A). Previously, CDK1 and DYRK1A were shown to facilitate TUBB3 phosphorylation at serine 172. Thus, we examined whether OSGIN1 knockdown may affect the interaction between TUBB3 and its upstream kinases. We found that OSGIN1 can bind with DYRK1A, but not CDK1 (Fig. 6B; Supplementary Fig. 6B). We then investigated the interaction between OSGIN1 and DYRK1A using recombinant proteins. Our results showed that OSGIN1 can directly bind with DYRK1A *in vitro* (Fig. 6C). We next examined whether the interaction between DYRK1A and OSGIN1 could affect the phosphorylation of TUBB3. We performed *in vitro* kinase assay and identified that OSGIN1 strongly

induced DYRK1A-mediated phosphorylation of TUBB3 at serine 172 (Fig. 6D). Therefore, we hypothesized that OSGIN1 can enhance the binding between TUBB3 and DYRK1A. We identified that the M3 region (1-342 amino acid fragment) of OSGIN1 was responsible for mediating the interaction with DYRK1A (Fig. 6E; Supplementary Fig. 6C).

To determine the binding mechanism of complexes (DYRK1A, TUBB3 and OSGIN1), we performed an *in vitro* binding assay using recombinant proteins. The results showed that OSGIN1 strongly enhanced the binding affinity between DYRK1A and TUBB3 (Fig. 6F). Additionally, to study the interaction between OSGIN1, TUBB3 and DYRK1A, we performed *in silico* docking using the HDOCK server [29]. Computer modeling further confirmed the interaction between OSGIN1, TUBB3, and DYRK1A (Fig. 6G). These results suggest that OSGIN1 may act as a scaffold protein to enhance binding of DYRK1A with TUBB3, thus reducing tubulin polymerization by regulating phosphorylation of TUBB3 at serine 172. Interestingly, knockdown of DYRK1A can deregulate OSGIN1 expression and also attenuate MKK3/6-p38 signaling pathway (Fig. 6H). Importantly, knockdown of OSGIN1 or TUBB3 did not affect DYRK1A expression levels (Supplementary Fig. 6D, E).

Suppression of OSGIN1 expression increases gefitinib sensitivity via the MKK3/6-p38 signaling pathway

It was previously reported that TUBB3 can promote anoikis resistance in NSCLC; therefore, we measured OSGIN1 and TUBB3 expression levels in gefitinib resistant HCC827R NSCLC cells. Our results showed that OSGIN1, TUBB3, and p-TUBB3 are all highly expressed in HCC827R cells when compared with gefitinib sensitive HCC827 cells (Supplementary Fig. 7A). We next performed MTT and foci formation assays to investigate the effect of OSGIN1 knockdown on gefitinib treated HCC827R cell growth. Results showed that OSGIN1 knockdown sensitized gefitinib resistant cells to different concentrations of gefitinib (Fig. 7A, B). Next, we conducted a MTT assay to analyze cell viability. OSGIN1 depletion decreased the viability of HCC827R cells, and gefitinib treatment resulted in robust inhibition of gefitinib resistant cell viability (Supplementary Fig. 7B, C). Moreover, similar alterations in cell viability were observed upon gefitinib treatment of TUBB3 knockdown HCC827R cells (Fig. 7C; Supplementary Fig. 7D). We then assessed whether depletion of OSGIN1 could result in decreased *in vivo* tumor growth using PDX murine models. PDX mice harboring gefitinib resistant tumors were assigned randomly to the following experimental groups: (1) shControl + Vehicle, (2) shControl + 50 mg/kg gefitinib, (3) shOSGIN1 #2 + Vehicle, (4) shOSGIN1 #2 + 50 mg/kg gefitinib. The gefitinib treatment regimen was initiated when the tumor volume reached approximately 300 mm³. Gefitinib or vehicle (5% DMSO in 10% tween 80) was orally administered by oral gavage once a day Monday through Friday. The volume and growth rate of tumors in shOSGIN1 #2 + 50mg/kg gefitinib mice were significantly decreased compared to shOSGIN1 #2 + Vehicle mice (Fig. 7D); however, the average body weight of mice did not differ significantly between the different groups (Supplementary Fig. 7E). The tumor sizes in the shOSGIN1 #2 group were significantly smaller than those in the shControl and shControl + Vehicle mice group (Fig. 7E). Intriguingly, the final average tumor weight in shOSGIN1 #2 + 50 mg/kg gefitinib mice groups was also reduced

compared to the weights of the shOSGIN1 #2 + Vehicle mice group (Fig. 7F). Western blotting analysis of tumor tissues confirmed lower OSGIN1 expression levels in tumor tissues with a lower growth rates via deregulation of MKK3/6-p38 signaling (Fig. 7G). These results strongly suggest that OSGIN1 plays an important role in tumor progression and gefitinib resistance.

Discussion

Since the discovery of OSGIN1 in 2001 [30], its biological function in normal cells has remained largely uncharacterized. Furthermore, details regarding the role of OSGIN1 in NSCLC development are even more limited. In this study, we identified a functional interaction between OSGIN1 and TUBB3 that is critical for regulating microtubule dynamics associated with lung tumor progression and gefitinib resistance. Specifically, using NSCLC PDX murine models and gefitinib resistant PDX murine models, we demonstrated a physiological role of OSGIN1 in the modulation of lung cancer growth and gefitinib resistance. Knock down of OSGIN1 in the lung cancer cell lines and patient-derived tumors that initially exhibited gefitinib resistance resulted in decreased lung tumor growth and the re-establishment of gefitinib sensitivity *in vitro* and *in vivo* (Fig. 2 and Fig. 7). Here, we suggest that OSGIN1 may act as a potential tumor promoter that enhances tumor growth and gefitinib resistance in NSCLC.

Elevated expression of TUBB3 has been observed in multiple malignancies and is associated with resistance to microtubule-targeting agents, tumor aggressiveness, and poor patient outcome [13, 18, 31]. TUBB3 was reported to promote tumorigenesis and anoikis resistance through PTEN/AKT signaling in NSCLC [19]. Understanding the mechanisms regulating TUBB3 function in NSCLC cancers is vital to develop strategies against TUBB3 overexpressing tumors. We conducted biochemical studies to illustrate that OSGIN1 did not regulate TUBB3 protein expression in NSCLC (Fig. 6A). However, we found that OSGIN1 regulated microtubule dynamics by modulating the phosphorylation of TUBB3 at serine 172 (Fig. 5A, 6A). Many studies have demonstrated that the modulation of microtubule dynamics significantly influences tumorigenesis and EGFR TKI resistance [24, 32, 33]. Microtubule dynamics play an important role in cell proliferation insofar that excessively rapid dynamics and suppressed dynamics induces mitotic block and spindle abnormalities and inhibit proliferation [34]. For example, it is well known that therapeutically targeting tubulin represents a potential effective means to treat aggressive cancers [35]. However, there are no reported inhibitors able to directly target TUBB3. Since targeting the complex network of protein-protein interactions (PPIs) has now been widely recognized as an attractive means to therapeutically manage cancer progression [36], we suggest that a TUBB3 PPI modulator may provide a novel strategy for the treatment of gefitinib resistant NSCLCs. Likewise, we propose that interventions which control microtubule dynamics by targeting OSGIN1 may increase favorable outcomes when treating drug resistant NSCLCs.

Dual specificity tyrosine phosphorylation regulated kinase 1A (DYRK1A) was reported to phosphorylate any β -tubulin isotype at serine 172 [37]. Importantly, phosphorylation of TUBB3 at serine 172 precludes the incorporation of tubulin dimers into microtubules, thus downregulating microtubule polymerization [21]. We found that OSGIN1 can enhance phosphorylation of TUBB3 at serine 172 by DYRK1A (Fig. 6D)

and binding of TUBB3 and DYRK1A (Fig. 6F). This finding is consistent with the results of a tubulin polymerization assay which showed that OSGIN1 knockdown enhanced tubulin polymerization (Fig. 5A, B). We speculated that OSGIN1 may function as a scaffold protein that promotes the interaction between DYRK1A and TUBB3, thus enhancing the phosphorylation of TUBB3 at serine 172. Numerous DYRK1A inhibitors were proven to be beneficial in treating several cancers and DYRK1A-related diseases [38, 39]; however, those inhibitors still need to be improved for clinical application due to nonspecific targeting [40]. Therefore, we suggest that PPI modulators may serve as a potential strategy to improve application of DYRK1A inhibitors. Additionally, we suggest that OSGIN1 may be a potential microtubule dynamics regulator in NSCLC.

EGFR TKIs resistance inevitably emerges over the course of disease management and remains a biological challenge [41]. Consequently, developing new treatment regimens that can overcome resistance are urgently needed [20]. In lung cancer, elevated TUBB3 expression has been shown to promote tumorigenesis, EMT, anoikis resistance, and gefitinib resistance [19, 20]. Microtubule-targeting agents (MTAs) constitute a diverse group of chemical compounds that bind to microtubules and affect their properties and function through modulating complex stability [42]. In our study, OSGIN1 knockdown was shown to stabilize microtubule polymerization by enhancing the phosphorylation of TUBB3 by DYRK1A. This finding suggests that modification of phosphorylation of TUBB3 by DYRK1A may provide a novel means to enhance MTA efficiency. Particularly, in gefitinib resistant NSCLC cells, targeting the IL-1 β /EHD1/TUBB3 axis was shown to circumvent resistance to EGFR-TKI by affecting microtubule dynamics [20]. Therefore, we strongly suggest that developing an modulator able to downregulate phosphorylation of TUBB3 by DYRK1A could be combined with EGFR inhibitors to overcome chemoresistance.

MKK3/6-p38 signaling plays a critical role in cell proliferation and TKI resistance in NSCLC [43, 44]. Previously, it was observed that phosphorylated p38 MAPK protein levels are strongly increased in lung cancer tissues compared with normal lung tissues, and treatment of lung cancer patients with p38 MAPK inhibitors has been shown to suppress lung tumor growth [45, 46]. Therefore, p38 MAPK pathways might be potential therapeutic targets in lung cancer. Accordingly, we verified that OSGIN1 knockdown inhibited p-MKK3/6 and p-p38 expression by phospho-proteomics and Western blotting (Fig. 5). It was previously reported that gefitinib could activate YAP-MKK3/6-p38 MAPK-STAT3 signaling and that the use of p38 MAPK inhibitors could eliminate gefitinib-induced tetraploidization and overcome gefitinib-resistance [24]. Accordingly, we showed that OSGIN1 and TUBB3 are highly expressed in gefitinib resistant cells. Moreover, OSGIN1 knockdown was shown to overcome gefitinib resistance *in vitro* and *in vivo*. Although the underlying mechanism responsible for regulating MKK3/6-p38 signaling through OSGIN1 or TUBB3 was not addressed in the present study, we will actively pursue this aspect in future investigations. Finally, we propose that interventions to control the expression of OSGIN1 may enhance the effectiveness of treating drug-resistant NSCLCs.

Conclusions

In conclusion, our current data suggests that OSGIN1 may act as a potential tumor promoter that enhances NSCLC growth and gefitinib resistance. OSGIN1 regulates microtubule dynamics by enhancing phosphorylation of TUBB3 by DYRK1A. Our present study reveals insights into the mode of action of OSGIN1 in NSCLC growth and gefitinib resistance *in vitro* and *in vivo*. Collectively, our findings suggest that OSGIN1 may serve as a potential marker protein that may be useful for the design of therapeutic strategies for gefitinib resistant NSCLCs.

Abbreviations

NSCLC non-small cell lung cancer

OSGIN1 Oxidative stress induced growth inhibitor 1

TUBB3 Tubulin beta 3 class III

DYRK1A Dual specificity tyrosine phosphorylation regulated kinase 1A

KEGG Kyoto encyclopedia of genes and genomes

MTT Methyl thiazolyl tetrazolium

IP Immunoprecipitation

MS Mass spectrometry

PDX Patient-derived lung tumor xenografts

Declarations

Ethics approval and consent to participate

Written informed consent was obtained from all subjects. All animal experiments were conducted in agreement with the Guide for the Care and Use of Laboratory Animals and approved by the Ethics Committee of Zhengzhou University (Zhengzhou, Henan, China).

Consent for publication

All authors agreed on the manuscript.

Availability of data and materials

The data are available to academic researchers upon request.

Competing interests

None of the authors have any competing interests.

Funding

This work was supported by National Natural Science Foundation China (NSFC) [grant number 82103193, 81802795, and 81872335]. Key Program of Henan Province, China [grant number 161100510300].

Authors' contributions

X.X. prepared the manuscript and performed the *in vitro*, the cell based and *in vivo* experiments; W. N. performed mass spectrometry, proteomics and phosphorproteomics analysis; J.L. performed computer modeling; K. V. L., Y. W. Y. and K. L. performed data analysis and manuscript editing; Y. S., Z.D. and D.J.K. supervised the overall experimental design and provided the idea.

Acknowledgements

We thank Xiangyu Wang for providing several plasmids. We are grateful to Dr. Xueli Tian for analysis of SPR and Ran Yang for preparation of immunohistochemical section.

References

1. Sung H, Ferlay J, Siegel RL, Laversanne M, Soerjomataram I, Jemal A, Bray F (2021) Global Cancer Statistics 2020: GLOBOCAN Estimates of Incidence and Mortality Worldwide for 36 Cancers in 185 Countries. *CA Cancer J Clin* 71:209–249. [10.3322/caac.21660](https://doi.org/10.3322/caac.21660)
2. Herbst RS, Morgensztern D, Boshoff C The biology and management of non-small cell lung cancer. *Nature* 2018, 553:446–54. [doi: 10.1038/nature25183](https://doi.org/10.1038/nature25183)
3. Molina JR, Yang P, Cassivi SD, Schild SE, Adjei AA Non-small cell lung cancer: epidemiology, risk factors, treatment, and survivorship. *Mayo Clin Proc* 2008, 83:584–94. [doi: 10.4065/83.5.584](https://doi.org/10.4065/83.5.584)
4. Filaire E, Dupuis C, Galvaing G, Aubreton S, Laurent H, Richard R, Filaire M (2013) Lung cancer: what are the links with oxidative stress, physical activity and nutrition. *Lung Cancer* 82:383–389. [10.1016/j.lungcan.2013.09.009](https://doi.org/10.1016/j.lungcan.2013.09.009)
5. Klaunig JE (2018) Oxidative Stress and Cancer. *Curr Pharm Des* 24:4771–4778. [10.2174/1381612825666190215121712](https://doi.org/10.2174/1381612825666190215121712)
6. Hu J, Yao H, Gan F, Tokarski A, Wang Y (2012) Interaction of OKL38 and p53 in regulating mitochondrial structure and function. *PLoS ONE* 7:e43362. [10.1371/journal.pone.0043362](https://doi.org/10.1371/journal.pone.0043362)
7. Ong CK, Leong C, Tan PH, Van T, Huynh H (2007) The role of 5' untranslated region in translational suppression of OKL38 mRNA in hepatocellular carcinoma. *Oncogene* 26:1155–1165. [10.1038/sj.onc.1209896](https://doi.org/10.1038/sj.onc.1209896)
8. Riou P, Saffroy R, Comoy J, Gross-Goupil M, Thiéry JP, Emile JF, Azoulay D, Piatier-Tonneau D, Lemoine A, Debuire B (2002) Investigation in liver tissues and cell lines of the transcription of 13

- genes mapping to the 16q24 region that are frequently deleted in hepatocellular carcinoma. *Clin Cancer Res* 8:3178–3186
9. Ong CK, Ng CY, Leong C, Ng CP, Foo KT, Tan PH, Huynh H (2004) Genomic structure of human OKL38 gene and its differential expression in kidney carcinogenesis. *J Biol Chem* 279:743–754. 10.1074/jbc.M308668200
 10. Liu M, Li Y, Chen L, Chan TH, Song Y, Fu L, Zeng TT, Dai YD, Zhu YH, Li Y et al (2014) Allele-specific imbalance of oxidative stress-induced growth inhibitor 1 associates with progression of hepatocellular carcinoma. *Gastroenterology* 146:1084–1096. 10.1053/j.gastro.2013.12.041
 11. Wang G, Zhou H, Strulovici-Barel Y, Al-Hijji M, Ou X, Salit J, Walters MS, Staudt MR, Kaner RJ, Crystal RG Role of OSGIN1 in mediating smoking-induced autophagy in the human airway epithelium. *Autophagy* 2017, 13:1205–20.doi: 10.1080/15548627.2017.1301327
 12. Khoi CS, Xiao CQ, Hung KY, Lin TY, Chiang CK (2022) Oxidative Stress-Induced Growth Inhibitor (OSGIN1), a Target of X-Box-Binding Protein 1, Protects Palmitic Acid-Induced Vascular Lipotoxicity through Maintaining Autophagy. *Biomedicines*. 10.doi:10.3390/biomedicines10050992
 13. Mariani M, Karki R, Spennato M, Pandya D, He S, Andreoli M, Fiedler P, Ferlini C (2015) Class III β -tubulin in normal and cancer tissues. *Gene* 563:109–114. 10.1016/j.gene.2015.03.061
 14. Borys F, Tobiasz P, Poterała M, Krawczyk H Development of novel derivatives of stilbene and macrocyclic compounds as potent of anti-microtubule factors. *Biomed Pharmacother* 2021, 133:110973.doi: 10.1016/j.biopha.2020.110973
 15. Tangutur AD, Kumar D, Krishna KV, Kantevari S Microtubule Targeting Agents as Cancer Chemotherapeutics: An Overview of Molecular Hybrids as Stabilizing and Destabilizing Agents. *Curr Top Med Chem* 2017, 17:2523–37.doi: 10.2174/1568026617666170104145640
 16. Hinsch A, Chaker A, Burdelski C, Koop C, Tsourlakis MC, Steurer S, Rink M, Eichenauer TS, Wilczak W, Wittmer C et al (2017) β III-tubulin overexpression is linked to aggressive tumor features and genetic instability in urinary bladder cancer. *Hum Pathol* 61:210–220. 10.1016/j.humpath.2016.11.005
 17. Ti SC, Pamula MC, Howes SC, Duellberg C, Cade NI, Kleiner RE, Forth S, Surrey T, Nogales E, Kapoor TM (2016) Mutations in Human Tubulin Proximal to the Kinesin-Binding Site Alter Dynamic Instability at Microtubule Plus- and Minus-Ends. *Dev Cell* 37:72–84. 10.1016/j.devcel.2016.03.003
 18. Kanakkanthara A, Miller JH β III-tubulin overexpression in cancer: Causes, consequences, and potential therapies. *Biochim Biophys Acta Rev Cancer* 2021, 1876:188607.doi: 10.1016/j.bbcan.2021.188607
 19. McCarroll JA, Gan PP, Erlich RB, Liu M, Dwarte T, Sagnella SS, Akerfeldt MC, Yang L, Parker AL, Chang MH et al (2015) TUBB3/ β III-tubulin acts through the PTEN/AKT signaling axis to promote tumorigenesis and anoikis resistance in non-small cell lung cancer. *Cancer Res* 75:415–425. 10.1158/0008-5472.Can-14-2740
 20. Huang J, Lan X, Wang T, Lu H, Cao M, Yan S, Cui Y, Jia D, Cai L, Xing Y (2020) Targeting the IL-1 β /EHD1/TUBB3 axis overcomes resistance to EGFR-TKI in NSCLC. *Oncogene* 39:1739–1755. 10.1038/s41388-019-1099-5

21. Fourest-Lieuvin A, Peris L, Gache V, Garcia-Saez I, Juillan-Binard C, Lantez V, Job D (2006) Microtubule regulation in mitosis: tubulin phosphorylation by the cyclin-dependent kinase Cdk1. *Mol Biol Cell* 17:1041–1050. 10.1091/mbc.e05-07-0621
22. Janke C, Magiera MM (2020) The tubulin code and its role in controlling microtubule properties and functions. *Nat Rev Mol Cell Biol* 21:307–326. 10.1038/s41580-020-0214-3
23. Breilkopf SB, Asara JM Determining in vivo phosphorylation sites using mass spectrometry. *Curr Protoc Mol Biol* 2012, Chap.18: Unit18.19.1–27.doi:10.1002/0471142727.mb1819s98
24. Yeung YT, Yin S, Lu B, Fan S, Yang R, Bai R, Zhang C, Bode AM, Liu K, Dong Z (2018) Losmapimod Overcomes Gefitinib Resistance in Non-small Cell Lung Cancer by Preventing Tetraploidization. *EBioMedicine* 28:51–61. 10.1016/j.ebiom.2018.01.017
25. Chandrashekar DS, Karthikeyan SK, Korla PK, Patel H, Shovon AR, Athar M, Netto GJ, Qin ZS, Kumar S, Manne U et al UALCAN: An update to the integrated cancer data analysis platform. *Neoplasia* 2022, 25:18–27.doi: 10.1016/j.neo.2022.01.001
26. Gyórfy B, Surowiak P, Budczies J, Lánczky A (2013) Online survival analysis software to assess the prognostic value of biomarkers using transcriptomic data in non-small-cell lung cancer. *PLoS ONE* 8:e82241. 10.1371/journal.pone.0082241
27. Kanehisa M, Sato Y, Kawashima M (2022) KEGG mapping tools for uncovering hidden features in biological data. *Protein Sci* 31:47–53. 10.1002/pro.4172
28. Lánczky A, Gyórfy B (2021) Web-Based Survival Analysis Tool Tailored for Medical Research (KMplot): Development and Implementation. *J Med Internet Res* 23:e27633. 10.2196/27633
29. Yan Y, Tao H, He J, Huang SY (2020) The HDock server for integrated protein-protein docking. *Nat Protoc* 15:1829–1852. 10.1038/s41596-020-0312-x
30. Huynh H, Ng CY, Ong CK, Lim KB, Chan TW Cloning and characterization of a novel pregnancy-induced growth inhibitor in mammary gland. *Endocrinology* 2001, 142:3607–15.doi: 10.1210/endo.142.8.8297
31. Duly AMP, Kao FCL, Teo WS, Kavallaris M β III-Tubulin Gene Regulation in Health and Disease. *Front Cell Dev Biol* 2022, 10:851542.doi: 10.3389/fcell.2022.851542
32. Vona R, Mileo AM, Matarrese P Microtubule-Based Mitochondrial Dynamics as a Valuable Therapeutic Target in Cancer. *Cancers (Basel)* 2021,13.doi: 10.3390/cancers13225812
33. Zhang W, Cho WC, Bloukh SH, Edis Z, Du W, He Y, Hu HY, Hagen T, Falahati M (2022) An overview on the exploring the interaction of inorganic nanoparticles with microtubules for the advancement of cancer therapeutics. *Int J Biol Macromol* 212:358–369. 10.1016/j.ijbiomac.2022.05.150
34. Gonçalves A, Braguer D, Kamath K, Martello L, Briand C, Horwitz S, Wilson L, Jordan MA (2001) Resistance to Taxol in lung cancer cells associated with increased microtubule dynamics. *Proc Natl Acad Sci U S A* 98:11737–11742. 10.1073/pnas.191388598
35. Dhiman A, Sharma R, Singh RK Target-based anticancer indole derivatives and insight into structure–activity relationship: A mechanistic review update (2018–2021). *Acta Pharm Sin B* 2022, 12:3006–27.doi: 10.1016/j.apsb.2022.03.021

36. Cheng SS, Yang GJ, Wang W, Leung CH, Ma DL The design and development of covalent protein-protein interaction inhibitors for cancer treatment. *J Hematol Oncol* 2020, 13:26. doi: 10.1186/s13045-020-00850-0
37. Ori-McKenney KM, McKenney RJ, Huang HH, Li T, Meltzer S, Jan LY, Vale RD, Wiita AP, Jan YN (2016) Phosphorylation of β -Tubulin by the Down Syndrome Kinase, Minibrain/DYRK1a, Regulates Microtubule Dynamics and Dendrite Morphogenesis. *Neuron* 90:551–563. 10.1016/j.neuron.2016.03.027
38. Liu T, Wang Y, Wang J, Ren C, Chen H, Zhang J DYRK1A inhibitors for disease therapy: Current status and perspectives. *Eur J Med Chem* 2022, 229:114062. doi: 10.1016/j.ejmech.2021.114062
39. de Souza MM, Cenci AR, Teixeira KF, Machado V, Mendes Schuler MCG, Gonçalves AE, Paula Dalmagro A, André Cazarin C, Gomes Ferreira LL, de Oliveira AS, Andricopulo AD (2023) DYRK1A Inhibitors and Perspectives for the Treatment of Alzheimer's Disease. *Curr Med Chem* 30:669–688. 10.2174/0929867329666220620162018
40. Lindberg MF, Meijer L (2021) Dual-Specificity, Tyrosine Phosphorylation-Regulated Kinases (DYRKs) and cdc2-Like Kinases (CLKs) in Human Disease, an Overview. *Int J Mol Sci* 22. 10.3390/ijms22116047
41. Reita D, Pabst L, Pencreach E, Guérin E, Dano L, Rimelen V, Voegeli AC, Vallat L, Mascaux C, Beau-Faller M (2021) Molecular Mechanism of EGFR-TKI Resistance in EGFR-Mutated Non-Small Cell Lung Cancer: Application to Biological Diagnostic and Monitoring. *Cancers (Basel)* 13. 10.3390/cancers13194926
42. Čermák V, Dostál V, Jelínek M, Libusová L, Kovář J, Rösel D, Brábek J (2020) Microtubule-targeting agents and their impact on cancer treatment. *Eur J Cell Biol* 99:151075. 10.1016/j.ejcb.2020.151075
43. Ko JC, Chiu HC, Wo TY, Huang YJ, Tseng SC, Huang YC, Chen HJ, Syu JJ, Chen CY, Jian YT et al (2013) Inhibition of p38 MAPK-dependent MutS homologue-2 (MSH2) expression by metformin enhances gefitinib-induced cytotoxicity in human squamous lung cancer cells. *Lung Cancer* 82:397–406. 10.1016/j.lungcan.2013.09.011
44. Tung CL, Chiu HC, Jian YJ, Jian YT, Chen CY, Syu JJ, Wo TY, Huang YJ, Tseng SC, Lin YW (2014) Down-regulation of MSH2 expression by an Hsp90 inhibitor enhances pemetrexed-induced cytotoxicity in human non-small-cell lung cancer cells. *Exp Cell Res* 322:345–354. 10.1016/j.yexcr.2014.02.002
45. Greenberg AK, Basu S, Hu J, Yie TA, Tchou-Wong KM, Rom WN, Lee TC (2002) Selective p38 activation in human non-small cell lung cancer. *Am J Respir Cell Mol Biol* 26:558–564. 10.1165/ajrcmb.26.5.4689
46. Campbell RM, Anderson BD, Brooks NA, Brooks HB, Chan EM, De Dios A, Gilmour R, Graff JR, Jambrina E, Mader M et al (2014) Characterization of LY2228820 dimesylate, a potent and selective inhibitor of p38 MAPK with antitumor activity. *Mol Cancer Ther* 13:364–374. 10.1158/1535-7163.Mct-13-0513

Figures

Figure 1. A+B+C+D+E+F by DJKim

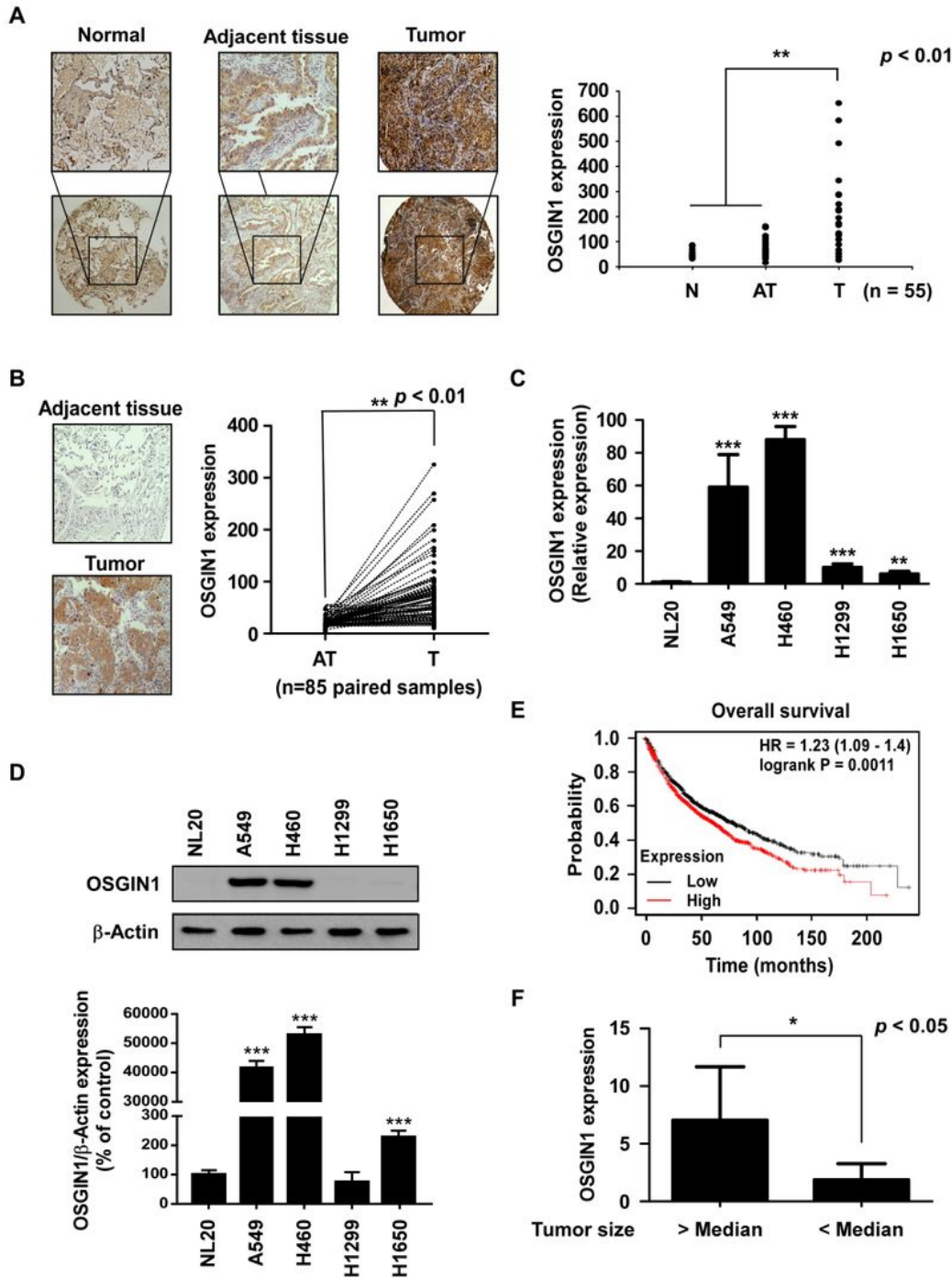


Figure 1

OSGIN1 is upregulated in non-small lung cancer and is associated with patients' overall survival. The expression of OSGIN1 in normal, adjacent and NSCLC tissues (A), and 85 paired NSCLC tissues (B) was analyzed by immunohistochemistry (N, normal; AT, adjacent tissue; T, cancer tissue). The expression of

OSGIN1 was determined using an inverted microscope; staining intensity was quantified using the Image-Pro PLUS (v.6) computer software program. Quantification of OSGIN1 protein expression is shown as a dot graph. (C) The mRNA expression of OSGIN1 in normal lung cells and NSCLC cells. The expression of OSGIN1 was analyzed by qRT-PCR. (D) The expression of OSGIN1 in normal lung cells and NSCLC cells. The expression of OSGIN1 was analyzed by Western blotting. (E, F) Clinical parameters of OSGIN1 expression in lung cancer patients. For E, overall survival was analyzed using the Kaplan–Meier plotter. For F, expression of OSGIN1 was analyzed in different tumor size of NSCLC patients by nonparametric test. The asterisks indicate a significant difference, * $p < 0.05$, ** $p < 0.01$, *** $p < 0.001$.

Figure 2. A+B+C+D+E+F+G by DJKim

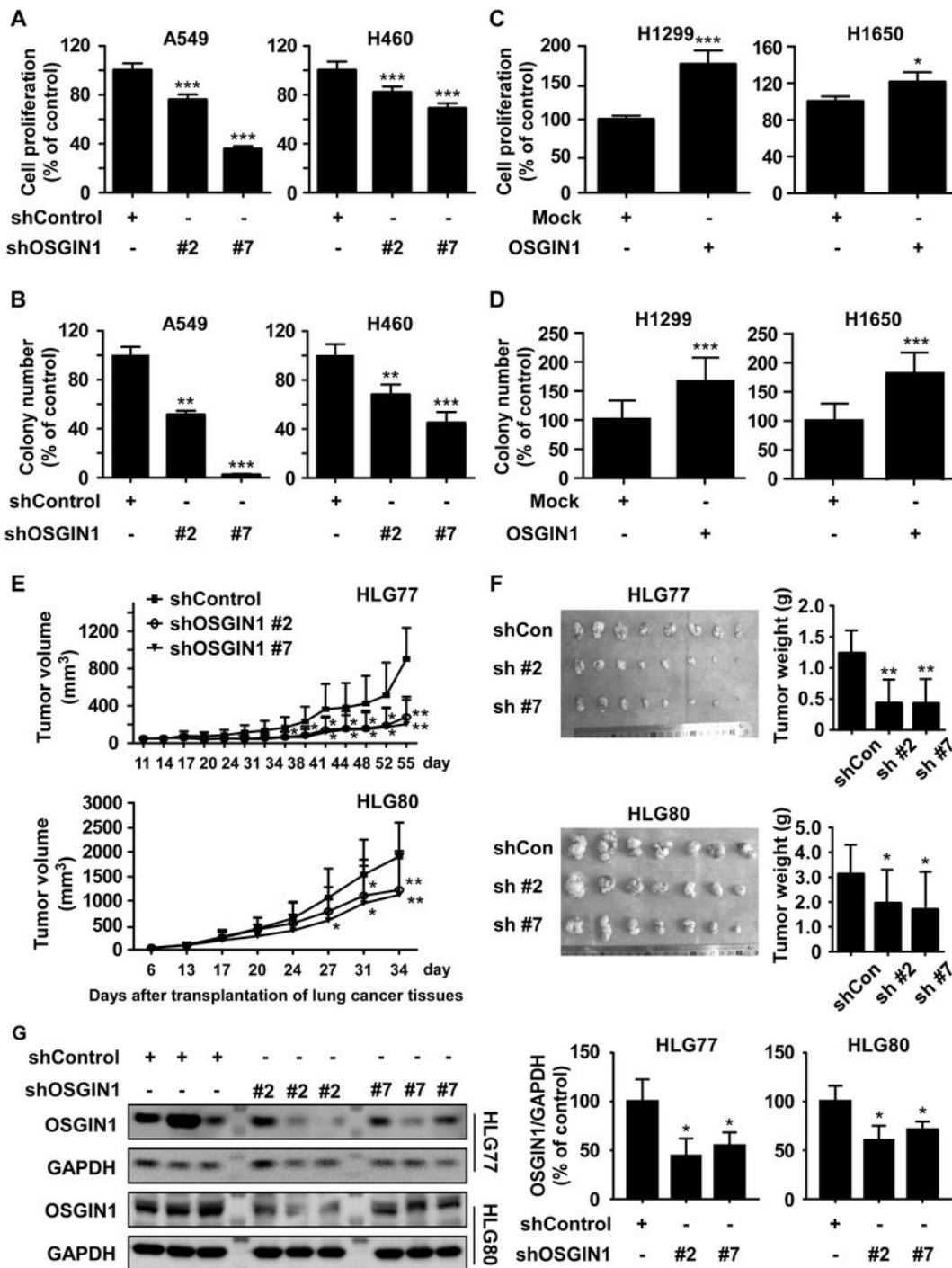


Figure 2

OSGIN1 promotes NSCLC growth *in vitro* and *in vivo*. (A, C) Effect of OSGIN1 knockdown or overexpression on cell proliferation was measured by MTT assay. (B, D) Anchorage-independent growth from different cells with OSGIN1 knockdown or overexpression. Colonies were counted using Image J-Plus. (E) Effect of OSGIN1 knockdown on NSCLC patient-derived xenograft tumor growth *in vivo*. Mice were divided into 3 groups as follows: 1) shControl group, 2) shOSGIN1 #2 group and 3) shOSGIN1 #7

group. NSCLC PDX tissues were treated by direct injection of each viral particle at three time points when the average tumor volume reached approximately 100 mm³. The tumor volumes of the HLG77 (upper panel) and HLG80 (lower panel) NSCLC PDX cases were measured on the indicated days. (F) Tumor photographs and relevant tumor weight. (G) Expression of OSGIN1 in PDX tumor tissues. Data from *in vitro* experiments were presented as means ±SD. All data statistical differences were evaluated using Student's t-test or one way ANOVA. * $p < 0.05$, ** $p < 0.01$, *** $p < 0.001$.

Figure 3. A+B+C+D by DJKim

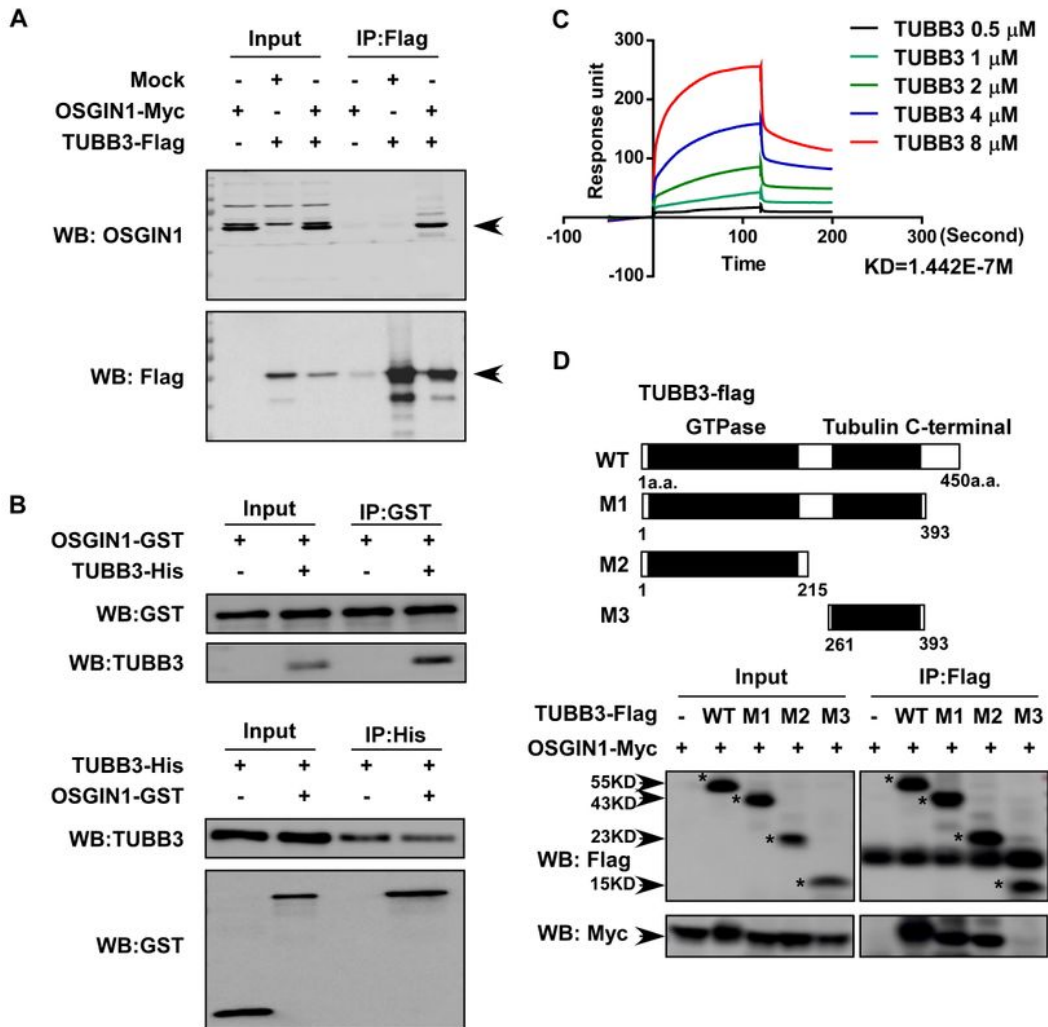


Figure 3

OSGIN1 directly interacts with TUBB3. (A) OSGIN1 interacts with TUBB3 in NSCLC cells. Cells expressing OSGIN1-myc and TUBB3-flag were immunoprecipitated using flag beads. The expression of flag and OSGIN1 was detected by Western blotting. (B) OSGIN1 directly interacts with TUBB3. Recombinant OSGIN1 and/or TUBB3 proteins were mixed and immunoprecipitated using GST beads or His beads. Binding between OSGIN1 and TUBB3 was detected by Western blotting. (C) SPR assay of OSGIN1 with TUBB3. OSGIN1 protein was immobilized on a CM5 sensor chip. Binding ability of different dose of TUBB3 with OSGIN1 were analyzed. (D) Truncated domain together with the amino acid number range for each domain of TUBB3 was shown in the upper. Flag immunoprecipitation (IP) from Lentix-293T cells expressing Myc-tagged OSGIN1 together with the different Flag-tagged TUBB3 domain mutants was shown in the bottom.

Figure 4. A+B+C+D+E+F+G by DJKim

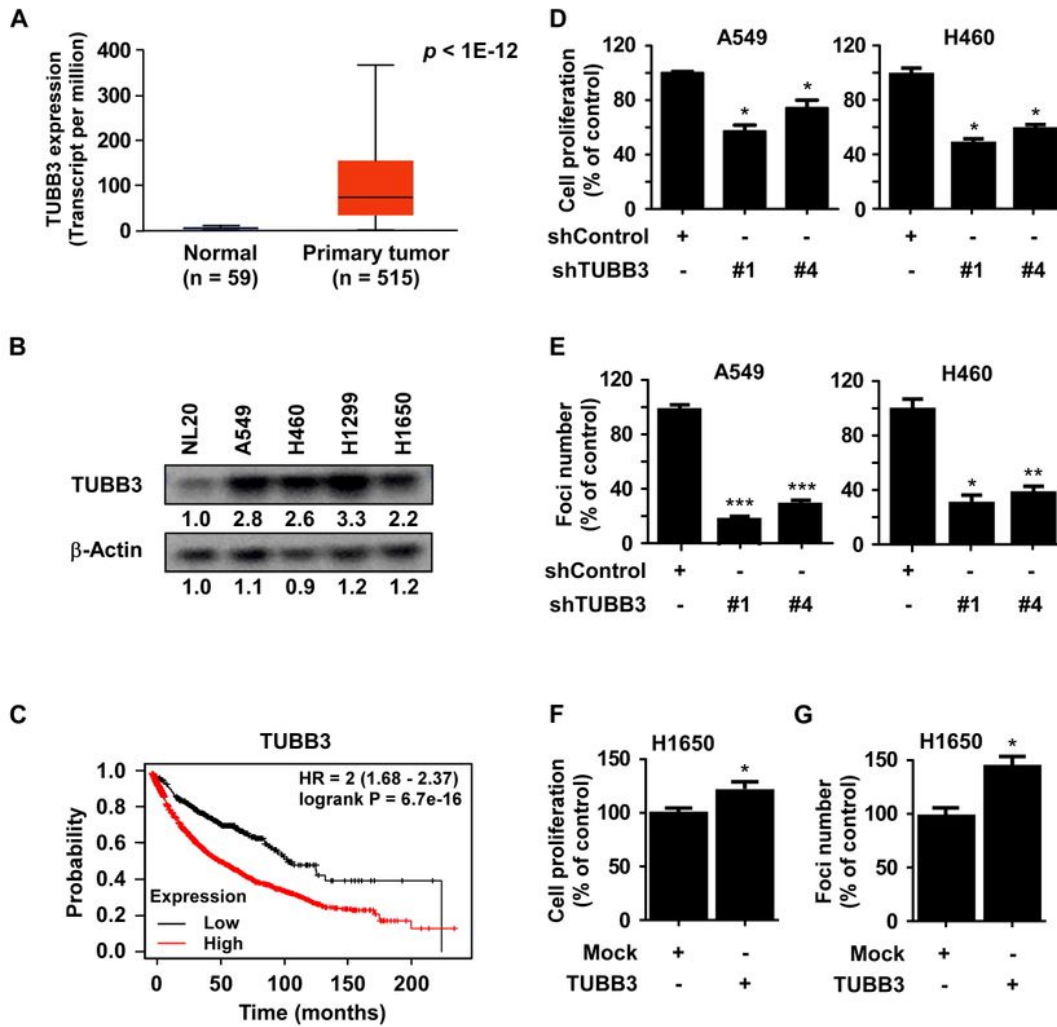


Figure 4

TUBB3 plays oncogenic effect on NSCLC. (A, C) Clinical parameters of OSGIN1 expression in lung cancer patients. For A, expression of TUBB3 in lung adenocarcinoma was analyzed by Ualcan database. For C, overall survival was analyzed using the Kaplan–Meier plotter. (B) The expression of TUBB3 in normal lung cells and NSCLC cells. The expression of TUBB3 was analyzed by Western blotting. (D, F) Cell proliferation in cells with TUBB3 knockdown or overexpression was measured by MTT assay. (E, G) Foci

formation in cells with TUBB3 knockdown or overexpression. All data statistical differences were evaluated using Student's t test or one way ANOVA. * $P < 0.05$, ** $P < 0.01$, *** $P < 0.001$.

Figure 5. A+B+C+D+E+F by DJKim

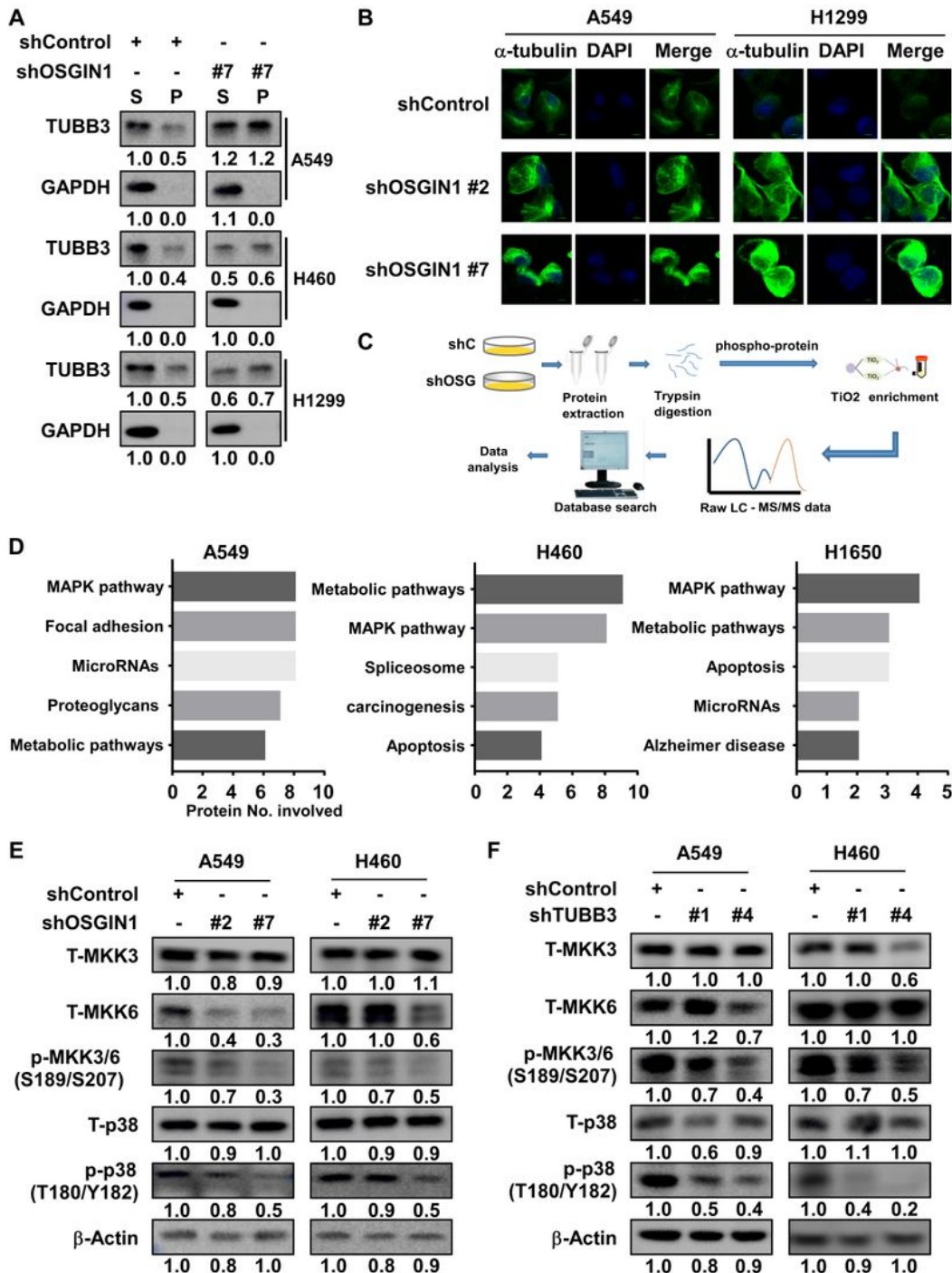


Figure 5

Suppression of OSGIN1 increases precipitate TUBB3 and repressing MKK3/6-p38 signaling pathway. (A) Tubulin polymerization assay to measure soluble and precipitated TUBB3. (B) Immunofluorescence

staining to check microtubule morphology in control and OSGIN1 knockdown cells. (C) Procedure for proteomics and phosphor-proteomics. (D) KEGG enrichment analysis according to proteomics and phosphor-proteomics. (E) MKK3/6-p38 signals in NSCLC cells expressing stable shOSGIN1. (F) MKK3/6-p38 signals in NSCLC cells expressing stable shTUBB3.

Figure 6. A+B+C+D+E+F+G+H by DJKim

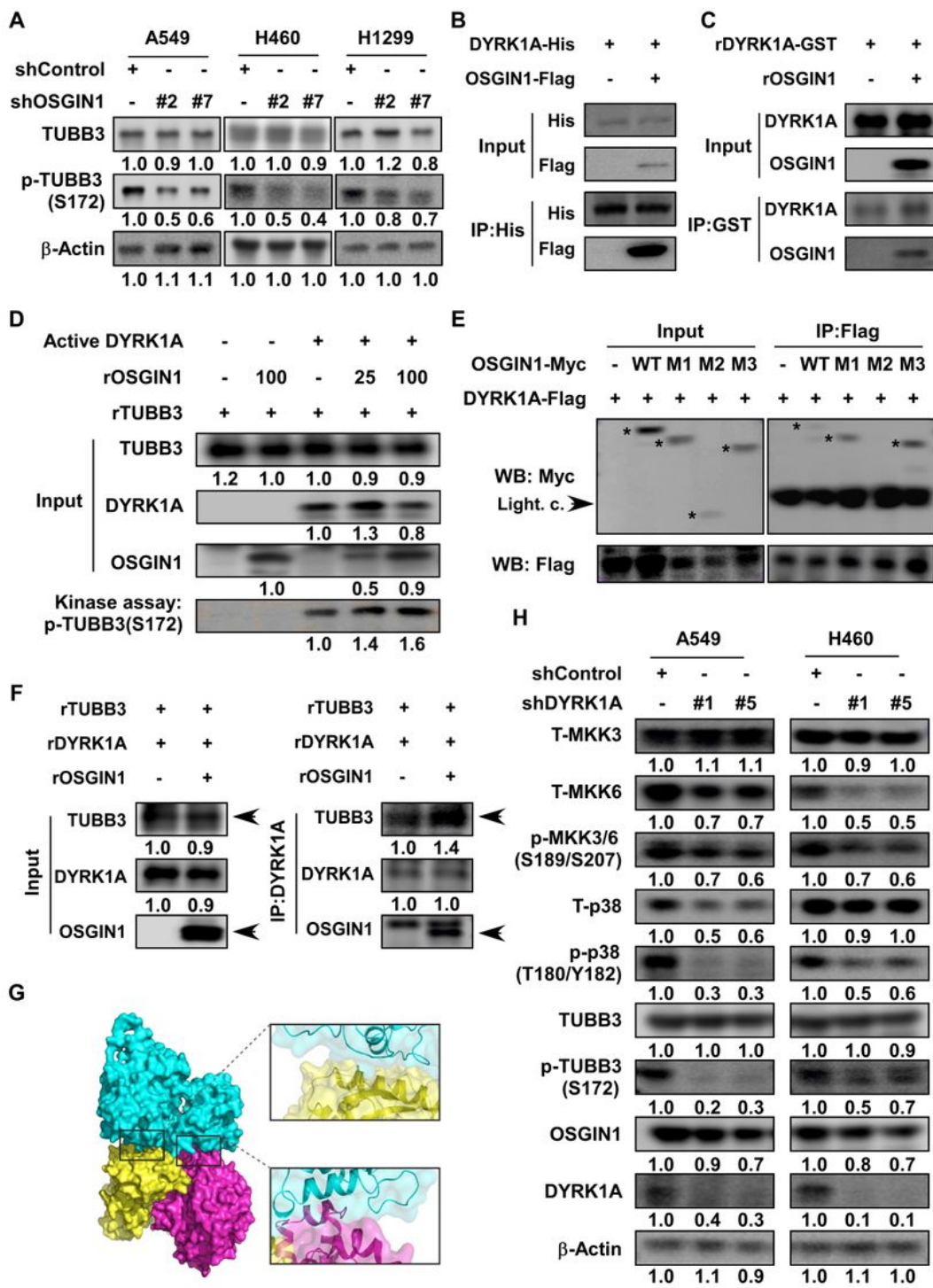


Figure 6

OSGIN1 promote phosphorylation of TUBB3 at serine 172 by DYRK1A via enhance interaction of DYRK1A and TUBB3. (A) The expression of TUBB3 and p-TUBB3 in control and OSGIN1 knockdown cells. The expression of TUBB3 and p-TUBB3 was measured by Western blotting. (B) OSGIN1 interacts with DYRK1A in NSCLC cells. Cells expressing OSGIN1-flag and DYRK1A-his were immunoprecipitated using his beads. The expression of flag and his was detected by Western blotting. (C) OSGIN1 interacts with DYRK1A *in vitro*. Recombinant OSGIN1 and/or DYRK1A proteins were mixed and immunoprecipitated using GST beads. Binding between OSGIN1 and DYRK1A was detected by Western blotting. (D) *in vitro* kinase assay to check effect of OSGIN1 on phosphorylation of TUBB3 by DYRK1A. (E) Flag immunoprecipitation (IP) from Lentix-293T cells expressing Flag-tagged DYRK1A together with the different Myc-tagged OSGIN1 domain mutants. (F) OSGIN1 enhances the interaction between TUBB3 and DYRK1A. Recombinant TUBB3 and DYRK1A proteins were co-incubated with or without OSGIN1 protein. Incubated proteins were immunoprecipitated using an anti-DYRK1A antibody. TUBB3, OSGIN1 and DYRK1A proteins were detected by Western blotting. (G) Modeling of OSGIN1 bind with TUBB3 and DYRK1A. Blue: OSGIN1; yellow: DYRK1A; Pink: TUBB3. The three-dimensional (3D) structures of TUBB3 and DYRK1A are derived from the Protein Data Bank (PDB Accession Number 6S8L and 2W06, respectively). DYRK1A catalytic residue Asp287 was specified to be within 8Å to the TUBB3 Ser172 in the docking process. The DYRK1A-TUBB3 model with the best docking score was chosen as the receptor molecule to further dock OSGIN1 into it. AlphaFold model (AF-Q9UJX0-F1-model_v4) of OSGIN1 was used. The final model is consistent with experimental data and has a docking score < -200, which is similar to the values of complex structures in the PDB, indicating a high-confidence model. (H) MKK3/6-p38 signals in NSCLC cells expressing stable shDYRK1A.

Figure 7. A+B+C+D+E+F+G by DJKim

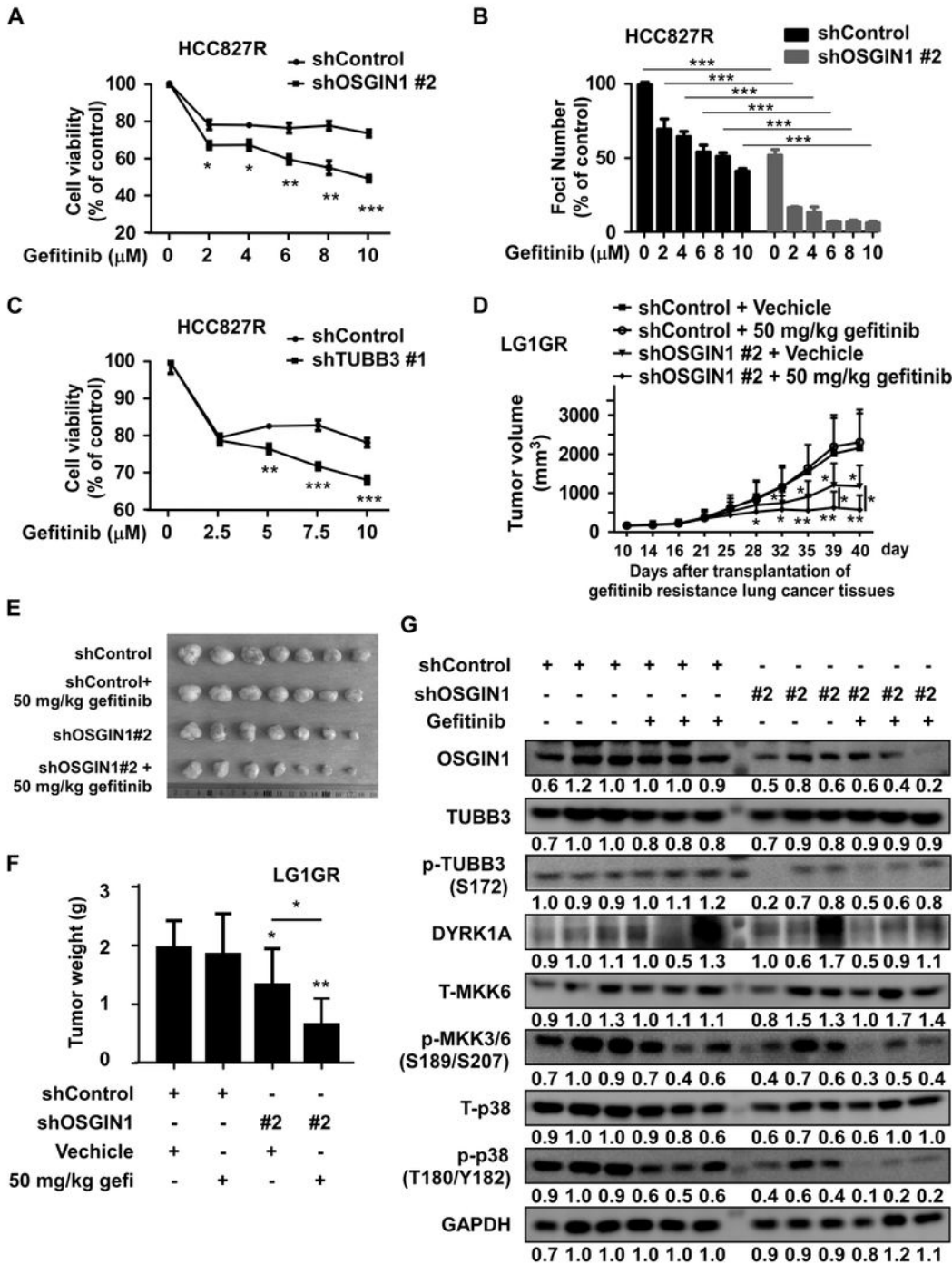


Figure 7

Suppression of OSGIN1 expression increases gefitinib sensitivity *in vitro* and *in vivo*. (A, C) HCC827R cells expressing shOSGIN1 or shTUBB3 and vector control cells were treated with the indicated doses of gefitinib for 48h, and cell viability was analyzed by MTT assay. (B) Foci formation of the indicated cells in the presence or absence of gefitinib was analyzed. (D) Effect of OSGIN1 knockdown on gefitinib resistant NSCLC patient-derived xenograft tumor growth *in vivo*. Mice were divided into 4 groups as follows: 1)

shControl + vehicle group, 2) shControl + 50 mg/kg gefitinib group, 3) shOSGIN1 #2 + vehicle group and 4) shOSGIN1 #2 + 50 mg/kg gefitinib group. Gefitinib resistant NSCLC PDX tissues were treated by direct injection of each viral particle at three time points when the average tumor volume reached approximately 100 mm³. And oral treatment for indicated gefitinib when the average tumor volume reached approximately 300 mm³. The tumor volumes of LG1GR NSCLC PDX cases were measured on the indicated days. (E) Tumor photographs. (F) Tumor weight. (G) Expression of OSGIN1 and MKK3/6-p38 signals in LG1GR NSCLC PDX tumor tissues. Data from *in vitro* experiments were presented as means \pm SD from triplicate experiments. All data statistical differences were evaluated using Student's t-test. * $P < 0.05$, ** $P < 0.01$, *** $P < 0.001$.

Figure 8. by DJKim

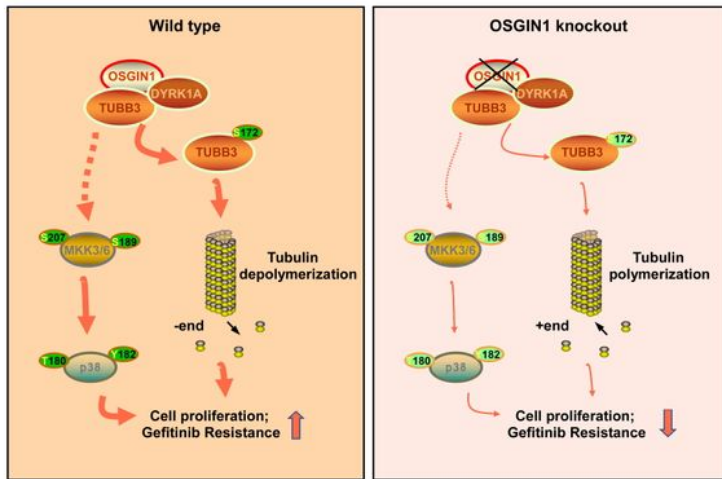


Figure 8

Schematic model for the findings of this work. Aberrant OSGIN1 in NSCLC binds TUBB3 and enhance phosphorylates TUBB3 at the S172 site by DYRK1A. Accumulated OSGIN1 upregulates the MKK3/6-p38 signals, which in turn contribute to NSCLC tumor growth and gefitinib resistance.

Supplementary Files

This is a list of supplementary files associated with this preprint. Click to download.

- [041023SupplementaryFigureLegend.docx](#)
- [SuppleFig1.jpg](#)
- [SuppleFig2.jpg](#)
- [SuppleFig3.jpg](#)
- [SuppleFig4.jpg](#)
- [SuppleFig5.jpg](#)
- [SuppleFig6.jpg](#)
- [SuppleFig7.jpg](#)
- [Supplementarytable1.xlsx](#)
- [Supplementarytable2.xlsx](#)